Applied Energy 426 (2026) 128538

Contents lists available at ScienceDirect

Applied Energy

journal homepage: www.elsevier.com/locate/apen

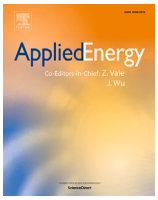

The significance of a polarization curve - analysis of a 60-cell polymer electrolyte water electrolysis stack

Eugen Hoppe*, Holger Janßen, Sebastian Holtwerth, Michael Hehemann, Walter Zwaygardt, Martin Müller

Forschungszentrum Jülich GmbH, Institute of Energy Technologies, IET-4, Wilhelm-Johnen-Straße, Jülich, 52428, NRW, Germany

HIGHLIGHTS

- Profound stack characterization using state-of-the-art sensors.
- Operation a stack with an active cell area > 1024 cm^2.
- Optimum stack efficiency, specific power consumption and thermal neutrality for the investigated stack at 0.6 Acm^{-2} and 1.6V.
- Strong correlation between contact resistance BPP-MEA and the corresponding cell voltage.
- Recombination catalyst enables safe stack operation even at very low current densities.

GRAPHICAL ABSTRACT

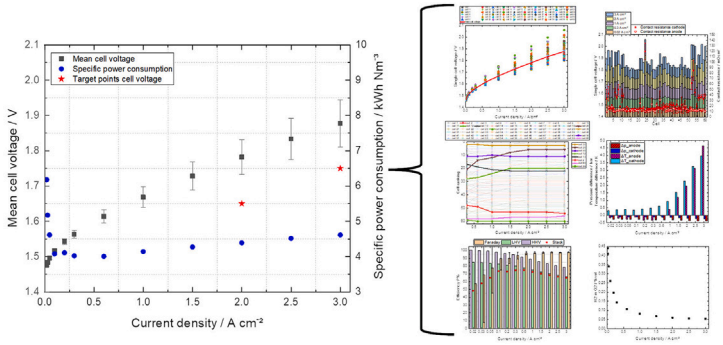

ARTICLE INFO

Keywords:
PEM water electrolysis
Industrially relevant stack size
Beginning-of-life characterization
Stack and Faraday efficiency
Specific power consumption
Thermoneutral operation

ABSTRACT

The objective of this study is to demonstrate the diversity of information encapsulated within a polarization curve and its operational boundary conditions. To this end, a polymer electrolyte membrane water electrolysis stack comprising 60 cells with an active cell area of 1024 cm^2 has been constructed and characterized. The performance data such as the average cell voltage of 1.88 V (η_{LHV} = 66.6 %) at the maximum applied current density of 3 A cm^{-2} and a minimum specific power requirement of 4.01 kWh m^{-3}_{N,H_2} at standard conditions at partial load (0.6 A cm^{-2}, η_{LHV} = 77.5 %) were extracted from the polarization curve. In addition, the current-dependent single cell voltage distributions, the pressure and temperature differences for the anode and cathode sides could be determined, as well as the Faraday and voltage efficiency. The maximum Faraday efficiency recorded, was 97.6 %. A significant finding was the measurement of an H_2 in O_2 concentration of 0.11 %vol at 0.6 A cm^{-2} which is far below the critical concentration of 4 %vol. Stack parameters and the begin-of-life state are determined based on the polarization curve and the supporting sensors.

1. Introduction

Höglinger et al. [1] provide a well-structured summary of the methods for characterizing an electrolyzer. These include, for example, hydraulic response curves, endurance runs, impedance measurements and cyclic voltammetry. According to Höglinger et al. [1], the last two methods are among the more advanced methods, but are unsuitable for stack characterization in terms of larger active cell areas. Lickert et al. [2] present a test protocol for a 4 cm^2 PEMWE single cell characterization including impedance measurements and polarization curves. In

* Corresponding author.
Email address: e.hoppe@fz-juelich.de (E. Hoppe).

https://doi.org/10.1016/j.apenergy.2026.128538
Received 19 March 2026; Received in revised form 25 June 2026; Accepted 26 July 2026
Available online 5 August 2026

literature, there are a few studies on electrolyzer stacks. Liebert et al. [3] were able to perform impedance measurements on a three-cell stack with 282 cm^2 active cell area. However, the focus was mainly on the middle cell. The end cells were largely not considered. Badwal et al. [4] used cells in the range of 9-100 cm^2. Smaller cell areas were used as single cells for the investigation of materials, design parameters and the variation of operating conditions. The 3-cell and 6-cell (each 50 cm^2) as well as the 2-cell and 14-cell (100 cm^2) stacks were used to determine polarization curves, efficiencies and degradation behavior. The 14-cell stack, operated at 80 °C, reached an efficiency of 86 $\%_{HHV}$ (73 $\%_{LHV}$) at 1 A cm^{-2}. Impedance measurements were only carried out for the smaller cell area. Badwal et al. [4] found that the mean contact resistance decreases with increasing cell number. The authors do not report a cell voltage distribution. As Badwal et al. [4] and Selamet et al. [5] also tested a stack up to 1 A cm^{-2} with an active cell area of 100 cm^2 but with 10 cells. The authors carried out both a temperature and a water flow variation. The temperature variation from 50 °C to 60 °C showed that the single cell performance improved by about 2 % points. The flow variation showed better performance at lower flow rates. For 50 °C at 1 A cm^{-2} the 5-cell stack showed an efficiency of 80 $\%_{HHV}$ (68 $\%_{LHV}$). The voltage spread at 1 A cm^{-2} is about 100 mV. Santarelli et al. [6] used the Giner GS-10 stack from Giner Electrochemical Systems LLC (US) consisting of twelve cells with a cell area of 160 cm^2 to validate a model at temperatures ranging from 42 °C to 58 °C and a pressure of up to 70 barg. In addition, the influence of stack temperature, cathode pressure, and water mass flow was analyzed, with the result that the voltage decreases with increasing temperature (5.25 mV $°C^{-1}$ at 7 barg), the voltage increases with increasing pressure (1.6 mV bar^{-1} at 60 °C). The stack achieves a specific power consumption of 5.39 kWh m^{-3}_{N,H_2} (index N: standard conditions 0 °C, 1013.25 mbar) at 70 barg at a maximum hydrogen production rate of 100 gh^{-1}. The authors concentrated more on the overall stack performance than on the single cell behavior. Hancke et al. [7] characterized a PEMWE system up to 180 bar differential pressure. The system comprises a 12 kW stack from Nel ASA with 34 cells and an active cell area of 90 cm^2. The authors showed a voltage efficiency of up to 71 $\%_{HHV}$ at 80 °C and 30 bar cathode pressure. The authors measured Faraday efficiencies between 99 % at 1.5 A cm^{-2} and 30 bar and 88 % at 1.86 A cm^{-2} and 50 bar. In terms of single cell voltages, a potential variation of less than ±1.54 % was achieved. Millet et al. [8] indicate an efficiency of almost 80 $\%_{HHV}$ (68 $\%_{LHV}$) for the tested commercial stack GenHy 1000 (twelve cells with 250 cm^2 each) for 1 A cm^{-2} and about 86 °C. The authors state the lowest specific energy consumption as 3.99 kWh m^{-3}_{N,H_2}. This was achieved with a current of 123.5 A and a stack voltage of 13.57 V at a temperature of 86 °C. In a single cell, the authors measured an H_2 in O_2 concentration of about 1.3 %vol at 6 barg with a current density of approximately 0.1 A cm^{-2} without a recombination catalyst layer. In a comparative study, Wang et al. [9] investigated an alkaline and a PEM stack from Shenzhen Hysear Technology Co., Ltd. (8 cells, 44.53 cm^2 electrode area, 360 W). The PEM stack reached a minimum specific power consumption of 4.01 kWh m^{-3}_{N} at 55 °C. The hydrogen in oxygen concentration was in the range of 2 %vol. In comparison to previous studies, Kimmel et al. [10] conducted degradation tests over 2200 h with a commercial stack consisting of 8 cells with an active cell area of 125 cm^2. Particularly noteworthy is that half of the cells were loaded with a total platinum group metals content of 2.4 $mgcm^{-2}$, while the other half were loaded with 3–3.5 $mgcm^{-2}$. This enabled the authors to investigate aging as a function of loading. Conditioning of the stack was done at 30 °C and 55 °C and current densities up to 2 and 4 A cm^{-2}, respectively. For the long-term test, no specific temperature is stated. For the impedance measurements, temperatures of 25 to 42 °C were chosen. The authors saw a performance increase after the 2000 h as the high-frequency-resistance decreased over time due to a membrane thinning. The authors state that they saw a hydrogen cross over increase, but do not quantify the hydrogen in oxygen concentration. Kimmel et al. [10] emphasized that this does not mean that there are no other degradation phenomena.

Table 1
Specification of the Greenlight Innovation test station G17-1560 [11].

Parameter	Maximum value
El. power	400 kW
Current	4000 A at 100 V
Voltage	125 V
Water supply (anode + cathode)	400 L min^{-1}
Hydrogen	2 m^3_N min^{-2} (0 °C, 1.013 bar)
Oxygen	1 m^3_N/min (0 °C, 1.013 bar)
Pressure (anode + cathode)	50 barg
Temperature	95 °C
Number cells	76

The existing literature has already demonstrated a certain extent of investigation into stack behavior. However, the dimensions of the cells and the total number of cells are not on an industrial scale. Additionally, there is a lack of attention paid to the individual cell voltages and the H_2 in O_2 behavior. In the present study, the aforementioned findings were demonstrated for a stack with a cell area of 1024 cm^2 and 60 cells, which corresponds to a maximum electrical output of approximately 350 kW. To the best of our knowledge, the individual studies typically conduct only sub-analyses. In this study, we present a wide-ranging analysis of a single industry-relevant stack.

2. Experimental

2.1. Test station

A test bench (G17-1560) developed in collaboration with Greenlight Innovation was used to characterize the stack. The specifications are given in Table 1. For further details, please refer to the process flow diagram in Ref. [11]. In addition to the current and voltage measurements, which also record the single cell voltages, other sensors have been integrated. The hydrogen concentration in the oxygen product line is measured continuously. On the one hand, this value is fundamental to the safety concept of the test station. On the other hand, it provides information about the efficiency of the stack's internal recombination catalyst layer as a part of the MEA. The amount of hydrogen produced and well as the temperatures and pressures at the input as output on the anode and cathode sides are also measured. Another important feature of the test bench is the ability to supply water to the anode only or to both the anode and cathode.

2.2. Sensors

The subsequent section will offer specific information on H_2 in O_2 concentration measurement and hydrogen mass flow measurement, along with the corresponding measurement accuracy. The focus is on these two sensors, as they are essential for safety and product gas determination. The H_2 in O_2 sensor must provide a reliable value so that the system is set to a safe state when a threshold value (in our case 40 % LEL) is reached. Since hydrogen is the main product of the electrolysis process, it is very important to know the mass flow rate accurately. This also allows the Faraday efficiency to be determined reliably.

2.2.1. H_2 in O_2 concentration

To measure the hydrogen in oxygen concentration a Messkonzept FTC300 sensor was used. The sensor in this case is a thermal conductivity sensor. Therefore, a two point calibration was performed. For both points, the gas was saturated with water with a dew point of 2 °C. For the zero point calibration pure oxygen was used, and for the end point calibration a premixed gas with a hydrogen in oxygen concentration of 2.02 %vol was used. During operation, the sample gas is extracted shortly

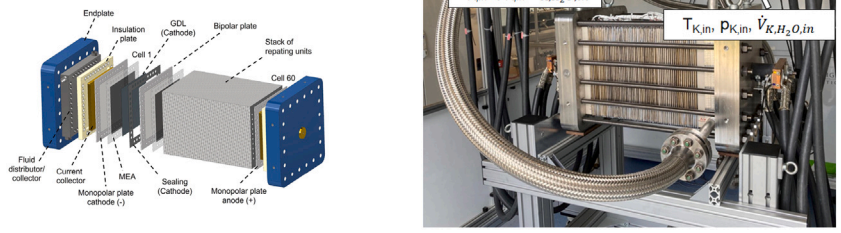

(a) (b)

Fig. 1. (a) Exploded view of the PEM electrolysis stack utilizing the novel bipolar plates. The outer stack dimensions are 0.58 m in height, 0.58 m in width, and 1 m in length and (b) the stack integrated into the test rig.

after its exit from the stack (anode), and the gas phase is separated from the liquid phase in a small separator. Subsequently, the gas is cooled down to a temperature of 2 °C prior to its entry into the sensor. The linearity of the sensor is less than 1 % of the range.

2.2.2. Hydrogen mass flow meter

For measuring the hydrogen mass flow the thermal mass flow meter Bronkhorst F116AI was used. For the specific sensor, the lowest accuracy during calibration was 0.3 % of the full scale (1800 $L_N\,min^{-2}$) which is equivalent to a hydrogen volume flow of 5.4 $L_N\,min^{-1}$. This results in deviations of more than 10 % for current densities lower than 0.1 $A\,cm^{-2}$ and deviations of less than 5 % for current densities above 0.3 $A\,cm^{-2}$. For the measurement, the gas is cooled down to a dew point of 20 °C which results in a water content of less than 0.5 % and is neglected in all further calculations.

2.3. Stack

Fig. 1 presents a 3D CAD drawing of our PEM type electrolysis stack in the form of an exploded view. The stack size assumes an electric power input of approximately 350 kW. Further technical details are shown in Table 2 and the CAD data can be found in Ref. [12]. The BPPs [13], MPPs, and CCM are designed for 1056 cm^2. In consideration of the thin membrane and manufacturing tolerances, the implementation of a subgasket was deemed necessary to prevent damage to the CCM. However, the implementation of this subgasket results in a reduction of the active cell area to 1024 cm^2.

The overall stack setup is fairly conventional. End plates and tension rods (not shown in Fig. 1) assist in stack clamping. A total of four pipes manage the water supply and gas/water mixture removal on the anode and cathode sides of the stack. A fluid distributor/collector, placed after one of the end plates, consists of four manifolds to distribute and collect the media streams at the stack level [14]. For more information on the stack mechanics, we refer to Ref. [15]. For safety reasons, the end plates are electrically isolated from the internal stack assembly. The technical implementation is a combination of isolation plate, made from PEEK, and an Au-plated Cu current collector plate. The latter consists of a flat plate as an inlay for the cutout of the insulation plate, with a massive bolt placed in the middle of it. Isolation plates, fluid distributor/collector, and end plates comprise corresponding holes to allow the current collectors' bolt to pass for an electric connection outside the stack. The diameter of the holes is significantly larger than the bolts' diameter to avoid electrical contact. In addition, isolating material is wrapped around the bolt. The stack assembly inside the previously described setup comprises the so-called repeating units. Each repeating unit consists of a Membrane Electrode Assembly (MEA), BPP (respect. BPP unit) and gaskets. More information on the CCM manufacturing and specification can be found in Refs. [11,16–18]. The only exception is that the internal stack assembly starts and ends with monopolar plates (MPP) that are conterminous to the current collector plates. Regarding the basic design layout of the BPP, it is beneficial if one can use a MPP instead with one side serving as the simple contact area towards the current collector plate. Two MPPs plus (n-1) BPPs, together with n MEAs constitute a stack with n cells (in our case n = 60). The CCM between the cathodic MPP and the first BPP is defined as cell number one, the cell sandwiched between the last BPP and the anodic MPP is then cell number 60. To reduce contact resistance at the Ti-PTL (anode) and expanded metal (cathode), the PTL was coated with Pt and the cathode with a graphene-like coating.

Table 2
Technical parameters of the stack and the performance target points for an operating temperature of 80 °C and atmospheric pressure. The target points represent performance data, achieved previously with a single test cell having an active area of 16 cm^2, conventional meander type flow field structure, and gold- respectively platinum-coated cathode and anode flow fields. The cell was operated at ambient pressure and a temperature of 80 °C.

Parameter	Value
Active cell area	1024 cm^2 (square-cut)
Number of cells	60
Nominal operating point (target)	1.65 V at 2 $A\,cm^{-2}$
Maximum operating point (target)	1.75 V at 3 $A\,cm^{-2}$
Maximum current (actual)	3072 A
Maximum stack voltage (actual)	113 V

2.4. Methods

2.4.1. Polarization curve

A polarization curve shows the actual electrical performance of a stack over the entire load range. The current/voltage dependency is recorded for a specified set of constant operating parameters. In principle, three different sections can be distinguished for increasing currents, which represent activation losses, ohmic losses and mass transport losses. Additional information about the performance of the stack can be obtained by displaying a series of polarization curves for different operating parameters. This is very helpful for identifying approaches for improvement. Plotting the current density instead of the total current over the average cell voltage allows comparison with other cells and stacks.

Polarization curves can be recorded either in potentiostatic or galvanostatic mode. In the first step, the pre-defined operational parameters on the anode and cathode sides are set:

- temperature at the stack inlet $T_{A,in}$ or outlet $T_{A,out}$.
- pressure at the stack inlet $p_{A,in}$ or outlet $p_{A,out}$.
- water flow rates $\dot{V}_{H_2O}$.
- hold time for each current or voltage step t_{hold}.

In a second step, the stack current or voltage is increased or decreased manually or automatically in stages. Stack responses (voltage/current but also the other parameters) are recorded at a defined frequency. In post processing, the current and voltage values for plotting the polarization curve are calculated (e.g., mean value during hold time, mean value of the last minute of hold time). In our case, 12 current density steps with a total hold time of 6.5 min each were chosen. The last five minutes were taken to calculate the average values. The time was chosen due to the behavior of the pressure regulation and the resulting fluctuating signal of the hydrogen volume flow. A complete steady state could not be achieved; however, the maximum standard deviations over the 5-minute observation period were approximately 3 mV for the single-cell voltages, 0.5 K for the inlet and outlet temperatures, and 40 mbar for the pressures. Therefore, we assumed a quasi-steady state.

2.4.2. Contact resistance measurement

Prior to the assembly of the stack, the contact resistance of the Ti-PTL on the anode and the expanded metal on the cathode was determined. To this end, the high-frequency resistance was measured using impedance spectroscopy. The PTL and expanded metal were then analyzed at four points using a gold-plated stamp and carbon paper (2 MPa contact pressure). On the cathode side, this corresponds to the actual structure in the stack.

2.4.3. Efficiencies

In addition to the pure description of the performance data of the stack in the form of a polarization curve, the efficiency of the stack is another important parameter for characterizing the quality of the stack. Depending on the focus, two efficiencies can be used. If the focus is on the hydrogen produced, the Faraday efficiency η_F, should be used (see Eq. (1)). This relates the actually usable hydrogen $\dot{m}_{H_2,measured}$ to the hydrogen $\dot{m}_{H_2,Faraday}$ theoretically produced according to Faraday's law.

$$\eta_F = \frac{\dot{m}_{H_2,measured}}{\dot{m}_{H_2,Faraday}} \tag{1}$$

In addition to Faraday efficiency, the performance of a cell can also be described by the voltage efficiency. In this case, the actual cell voltage E_{cell} is related to the theoretical potential required for water splitting (25 °C, 1.013 bar), which is based on the reaction enthalpy. The lower heating value (LHV) or the higher heating value (HHV) is used, depending on whether the water is in a gaseous state (η_{LHV}) or liquid (η_{HHV}). The efficiencies can be calculated using Eqs. (2) and (3).

$$\eta_{LHV} = \frac{1.25\,\mathrm{V}}{E_{cell}} \tag{2}$$

$$\eta_{HHV} = \frac{1.48\,\mathrm{V}}{E_{cell}} \tag{3}$$

3. Results

For the stack used here, the polarization curve averaged with respect to the number of cells is shown in Fig. 2. This was recorded at a stack input temperature of 70 °C on both the anode and cathode sides, a cathode input pressure of 5 barg, an anode input pressure of 4 barg, and a water flow rate of 123 L min^{-1} on each side. As described in Section 2.4.1, the total hold time per current density step was 6.5 min to stabilize the voltage signal. The last five minutes were used for evaluation. In a first step, the arithmetic mean cell voltage for each current density step, calculated from the stack voltage is shown in Fig. 2. Moreover, the target points for the potential are indicated by stars (see Table 2). With respect to the target values, a mean cell voltage of 1.78 V ± 0.05 V (±2.8 %) at a current density of 2 A cm^{-2} and a mean cell voltage of 1.88 V ± 0.07 V (±3.7 %) at a current density of 3 A cm^{-2} were achieved. The targeted potential, on the other hand, deviates by 130 mV for the maximum current density. The target point was achieved at atmospheric pressure and a cell temperature of 80 °C. The polarization curve recorded in this study was obtained at an anode and cathode pressure of 4 and 5 barg, respectively. A direct comparison is not possible since, for technical reasons, the operating conditions of the laboratory cell could not be matched to those of the 60-cell stack. Nevertheless, to provide some context, we attempted to calculate the impact of the deviation in the operating parameters. According to the Nernst-Equation, this pressure deviation accounts for at least a 30 mV deviation. The potential increase due to a 10 K lower temperature in comparison to the lab cell accounts as well for about 30 mV, based on the study of Moradi Nafchi et al. [19]. This means that almost half of the difference can be attributed to the different operating conditions.

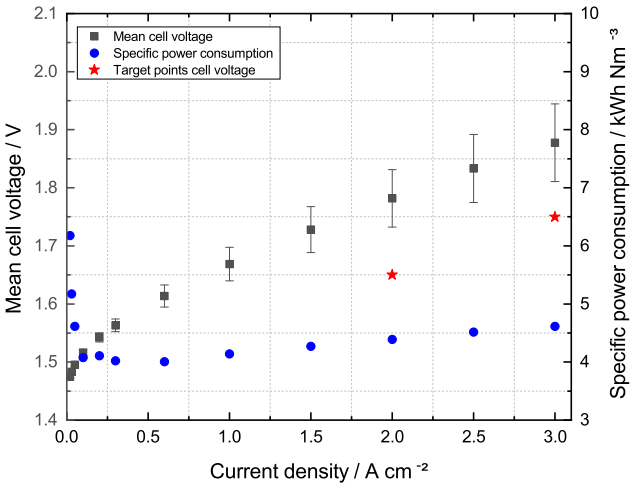

Fig. 2. Averaged single cell voltage for an inlet temperature of 70 °C on both sides, an inlet pressure of 4 barg at the anode and 5 barg at the cathode, and an inlet water flow of 123 L min^{-1} on both sides. Target points refer to 80 °C and atmospheric pressure.

Compared to the targets set by the U.S. Department of Energy, the stack exceeds the 2022 benchmark (2 A cm^{-2} at 1.9 V per cell) and, when compared to the 2026 targets, is slightly above the required single-cell voltage of 1.8 V at 3 A cm^{-2} [20]. For commercial stacks no UI data are available.

For an economic comparison of stacks, the specific power consumption ($U_{stack} \cdot I_{stack} \cdot \dot{V}_{H_2}^{-1}$) of the stack, i.e., how much electrical energy is required to produce one standard cubic meter of hydrogen, is of particular interest. This power consumption is also shown in Fig. 2. At the lowest measured current density of 0.02 A cm^{-2}, the specific power consumption is 6.18 kWh m^{-3}_{N,H_2}, which represents the maximum of the analyzed interval. As the current density increases, the power consumption drops to a minimum of 4.01 kWh m^{-3}_{N,H_2} at 0.6 A cm^{-2}. Subsequently, the specific power consumption increases to 4.5 kWh m^{-3}_{N,H_2} at the highest measured current density. Taking into account the error in the hydrogen volume flow measurement, the specific power consumption at 0.6 A cm^{-2} ranges from 3.93 kWh m^{-3}_{N,H_2} to 4.09 kWh m^{-3}_{N,H_2}. This curve can be easily explained based on the efficiency values (see Fig. 7). At low current densities, the loss of hydrogen due to crossover and leakages through gaskets is highest compared to the quantity produced. At high current densities, voltage efficiency has the greater influence. With these efficiency levels, the stack achieves efficiencies that commercial manufacturers also specify [21].

Regardless of the specific stack performance, the activation and ohmic regions can be clearly seen. In contrast, the area of mass transport limitation cannot be recognized at the highest current densities.

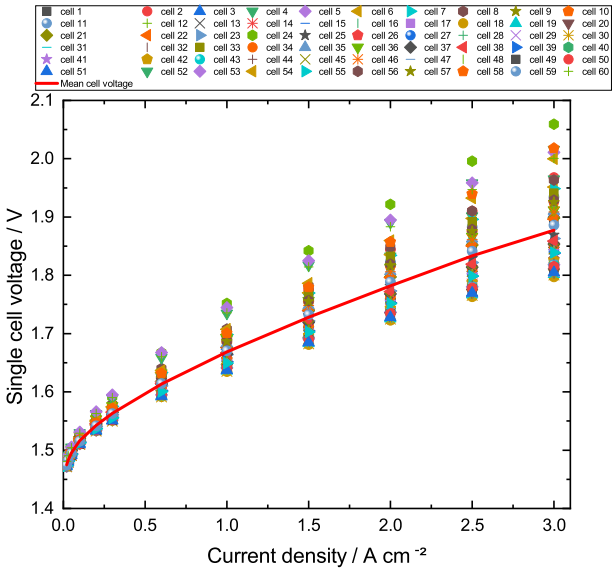

Fig. 3. Single cell voltages of all 60 cells in the stack including the arithmetic mean cell voltage.

However, it is not possible to generalize this to all cells. A single cell voltage measurement is required. Fig. 3 shows the averaged single cell voltage as a solid line and the single cell voltages as dots. It should be noted that the visualization does not claim to show all values in detail. Rather, the representation allows more global effects to be shown. First, the large spread of cell voltages can be seen, especially at high current densities. In the low current density range, the difference between the best and worst cell is 11 mV (0.02 A cm^{-2}), and at the highest measured current density of 3 A cm^{-2} it is 260 mV (1.8 V vs. 2.06 V). This means that the difference increases by a factor of 24 as the current density increases. Based on the Z-value used to identify outliers (Z > 2), four outliers are found for a current density of 3 A cm^{-2}. These are cells with No. 53, 52, 58, and 24. Excluding these cells, the average cell voltage would decrease by 10 mV to 1.86 V μ 0.06V, and the maximum spread decreases by approximately 60 mV to 202 mV.

As can already be seen in Fig. 2, there is an ohmic range with one slope. In Fig. 3, it can also be seen that the corresponding slope is not the same for all cells, which corresponds with the previously described voltage spread behavior. These different slopes can have various causes. A critical factor that is unique to stacks, is the reproducibility of the materials used, in particular the dimensional tolerance of the BPP and gaskets as well as the thickness of the PTLs. Using the same gasket thickness for all cells will result in different compression of the PTLs and therefore different electrical resistances [22]. In addition to the manufacturing tolerances of the PTLs, the coating of the Ti-PTL on the anode as well as the MPP and BPP is also of critical importance as it reduces the contact resistance between the individual layers and minimizes passivation of the layers. This can be explained above all by the different contact resistances of the bipolar plates. For this purpose, the contact resistance of the BPP and MPP was measured (see Section 2.4.2). There is a strong correlation (R^2 = 0.6) with the cathodic contact resistance, which is shown in Fig. 4 together with the cell voltage distribution for four current densities. Cell 24 is particularly striking, showing the highest voltage at all current densities. At the same time, the largest contact resistance of 119 mΩcm^2 was also measured for cell 24. The polarization curve can be used to classify the contribution of the cathode-side contact resistance of the BPP to the total ohmic resistance of cell 24. Between 1 and 2 A cm^{-2} the voltage increase is 170 mV. This results in a resistance of 170 mΩcm^2. Typically, the protonic resistance of the membrane has the largest share of the total ohmic resistance of an electrolytic cell. It is noteworthy that the conductivity or resistance of the membrane is challenging to measure in situ, given the size of the active cell area [1]. Consequently, it was assumed that the membrane has a constant resistance across the entire range. The conductivity of Nafion at 70 °C in liquid water is about 165 mScm^{-1} [23]. For the Nafion 212 used (thickness 50 μm), this results in a resistance of about 30 mΩcm^2. This means that the sum of the BPP contact resistance, and the membrane resistance corresponds to 88 % of the total resistance from the polarization curve. 70 % of the total resistance is accounted for by the contact resistance alone. A similar correlation can be observed for most of the other cells (see Fig. 4). As can be seen from the polarization curve, the cell voltage distribution becomes more inhomogeneous as the current density increases. From 1 to 2 A cm^{-2} the average cell voltage increase is 113 mV, and for cell 24 it is 50 % higher. The lowest increase is 88 mV for this current density change. A similar picture emerges for the other two current density changes. The cells which already showed the worst performance at low current densities show a higher increase in cell voltage with increasing current density. Due to the deviation from the standard conditions, some cells show a cell voltage below 1.48 V at a current density of 0.02 A cm^{-2}.

To further investigate the phenomenon of the different potential increase, the cells were systematically sorted based on their cell voltage for each current density. As illustrated in Fig. 5, the respective rank (y-axis) of each cell is depicted for the examined current densities (x-axis). The best cell, which has the lowest voltage at a specific current density, is shown as 1. The worst is in 60th place. To enhance the clarity of the figure, cells that exhibited particularly noteworthy behaviors were selected and highlighted. The figure reveals three distinct behaviors: Cells (i) that consistently have approximately the same ranking across the entire current density range (cells 24, 30, and 60). Additionally, cells (ii), such as numbers 12 and 20, exhibit higher cell voltages at low current densities compared to other cells. However, as current density increases, these cells demonstrate superior performance, exhibiting lower voltages. Finally, cells (iii) display an opposing trend. Initially, cells 13 and 2 exhibit lower cell voltages in the activation regime, but as current density increases, their performance deteriorates. It turns out that only one cell (cell 50) keeps its position. 52 % of the cells improve their position and 47 % get worse. This is partly due to the different ohmic resistances, which result in different slopes. This indicates that certain cells undergo a change in position by multiple increments, while others exhibit a change by a single increment. Consequently, the distribution does not align with a 50:50 ratio. On the other hand, some cells may already be better or worse than others in the activation area, causing a change in position at higher current densities.

The more system-relevant changes are shown in Fig. 6(a). Fig. 6(a) elucidates the pressure drop and temperature change (*outlet* − *inlet*) of the 2-phase flow across the stack for the anode and cathode sides. The data show that an increase in current density from 0.02 A cm^{-2} to 3 A cm^{-2} results in an increase in pressure drop on the anode and cathode sides of approximately 100 mbar for the same water flow rate. The pressure drop on the anode at the lowest current density was 300 mbar, and 120 mbar on the cathode side at an identical water flow rate of 123 L min^{-1}. The observed difference in pressure drop may be attributed to the varying porosity of the PTL utilized. The C-PTL exhibits an initial porosity that is approximately 10 percentage points higher than the Ti-PTL on the anode side, resulting in a lower flow resistance. The increased gas content in the 2-phase flow with increasing current density does not lead to any visible mass transport inhibition. Consequently, the gas can be efficiently removed from the cell and, by extension, the catalyst layer. Therefore, this suggests that every cell is sufficiently supplied with water. Given the large excess of water used for temperature control, a homogeneous distribution can be assumed. However, a more significant finding is the increase in the temperature difference from input to output. At current densities of up to 0.6 A cm^{-2}, the initial temperature increase is almost negligible. This is in good correlation to the specific heat generation due to the overpotential related to 1.48 V. As can be seen in Fig. 6, the produced heat is almost zero for low current densities. The

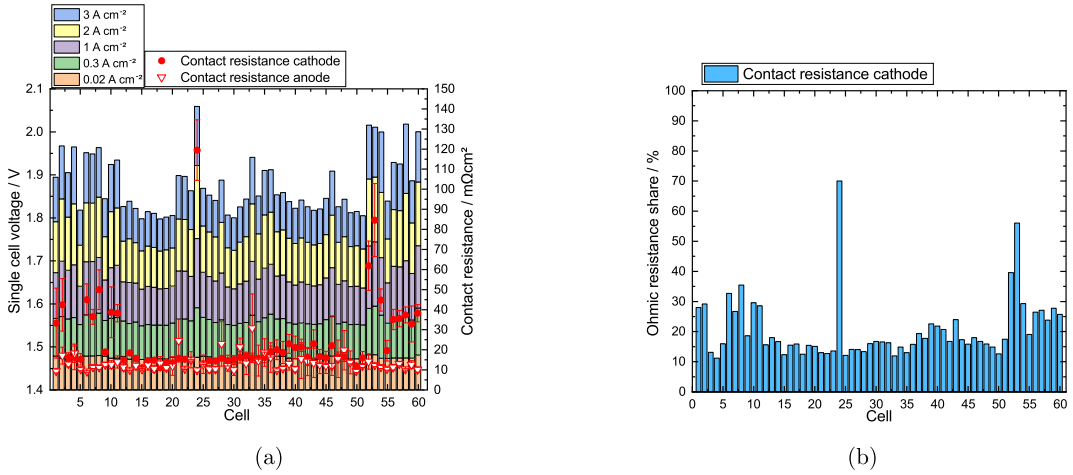

Fig. 4. (a) Single cell voltage distribution of all 60 cells of the stack for five different current densities and the cathodic and anodic contact resistances of the MPP and BPP, (b) the share of the cathodic contact resistance in the total ohmic resistance of the cell.

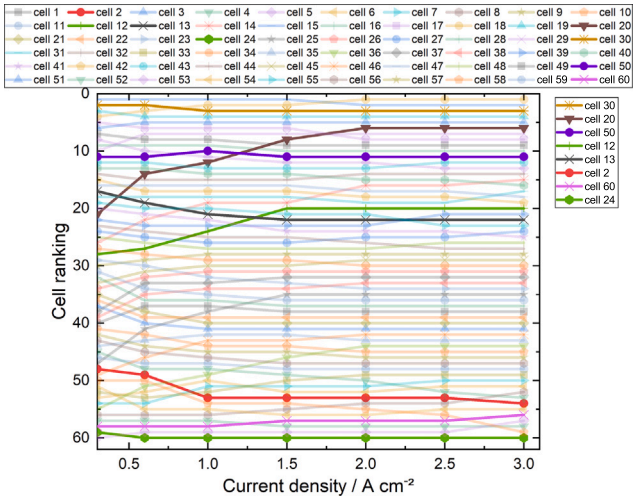

Fig. 5. Cell ranking of all 60 cells for the entire current density range.

temperature differences are in the range of approximately μ 0.5K and can be attributed to measurement uncertainties of the type K thermocouples used. At a current density of 1 A cm^{-2}, the temperature rises by approximately 1 K on the anode and cathode sides. At around 0.6 A cm^{-2} we can identify the thermoneutral operation of the stack. Therefore, the heat produced (due to electrochemical losses and the recombination of the permeated hydrogen) at 0.6 A cm^{-2}, compensates for the sum of the heat fluxes dissipated (convection to the outside, water heating, enthalpy of vaporization, etc.) (Fig. 6). Hence, no additional heating or cooling is required here. Below 0.6 A cm^{-2}, the measurements (within the accuracy range) indicate a cooling of the anode water mass flow. In this case, additional heating is necessary to achieve the required water inlet temperature. The temperature difference then increases continuously with increasing current density as the specific heat increases, reaching 4.8 K at 3 A cm^{-2}. This temperature increase does not exceed the 5 K limit stipulated by numerous manufacturers. Should the current density be increased further or the stack be degraded, the cell voltage would rise, resulting in an increase in the heat input into the stack. This would lead to a temperature difference that exceeds the 5 K threshold. To counteract this effect, the water mass flow would need to be augmented, thereby enabling the removal of additional heat from the stack.

As is well established, the electrolysis process is subject to various losses that increase the voltage required for the water splitting process, accompanied by a reduction in efficiency. As previously mentioned in chapter Section 2.4.3, two types of efficiency are useful to characterize electrolysis stacks: voltage efficiency and Faraday efficiency. In the case of voltage efficiency, the actual cell voltage can be related to both the LHV and the HHV. The bar chart in Fig. 7 shows all three efficiencies for the entire current density range examined. It should be noted that, for the sake of completeness, the Faraday efficiencies for current densities below 0.1 A cm^{-2} are also shown; however, their interpretive value is limited due to the high level of uncertainty inherent in the data. This is further corroborated by the error bars plotted on the chart. At the lowest measured current density of 0.02 A cm^{-2}, the voltage efficiency was 84.8 %$_{\mathrm{LHV}}$. Due to the deviation from the standard conditions, the efficiency in terms of the HHV can reach values above 100 %. However, with increasing current density and the associated increasing losses, both voltage efficiencies decrease reaching a value of 66.7 %$_{\mathrm{LHV}}$ and 78.8 %$_{\mathrm{HHV}}$ at 3 A cm^{-2}. Conversely, Faraday efficiency demonstrates the opposite behavior. The efficiency increases with rising current density, reaching 97.6 % at 3 A cm^{-2}. Despite the linear increase in hydrogen permeation flux with increasing current density [24], the ratio of permeation flux to hydrogen produced decreases. Considering efficiencies separately, different optimal operating points are identified. In accordance with Faraday efficiency, high current densities must be selected to achieve the highest hydrogen yield. In terms of voltage efficiency, however, the lowest possible current must be selected. Nevertheless, the amount of hydrogen produced would be minimal, and stack operation would probably be uneconomical. Therefore, the stack efficiency $\eta_{stack} = \eta_F \cdot \eta_{LHV}$ can also be considered. For the specific stack employed, its performance reaches its optimal level at a current density of 0.6 A cm^{-2}, yielding an efficiency of 74.9 %. Conversely, the specific power consumption is observed to be at its minimum at 0.6 A cm^{-2} at 4 kWh m$^{-3}_{\mathrm{N,H_2}}$ as can be seen from Fig. 2. Furthermore, at this operating point, the stack does not need to be cooled or heated, as already shown in Fig. 6(a). In addition, this optimal operating point with an average cell voltage of 1.6 V coincides with the findings of Scheepers et al. [25], who recommend an optimal cell voltage of approximately 1.62 V for a stack at equal pressure and 70 °C operating temperature. The present study enabled the validation of the theoretical considerations and the model from Scheepers et al. [25] at an industry-relevant scale.

Assuming that the hydrogen loss increases or decreases at the same rate for all current densities, the optimal current density would still be 0.6 A cm^{-2}, since this would only cause a parallel shift in the Faraday efficiency. Thus, the optimal operating point would not change. Insulating

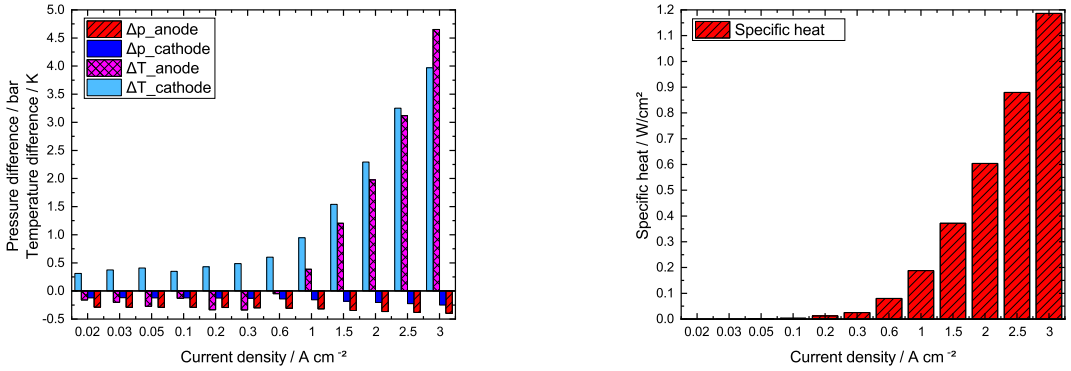

(a) (b)

Fig. 6. (a) Pressure and temperature changes from stack inlet to outlet with an inlet temperature of 70 °C on both sides, an inlet pressure of 4 barg at the anode and 5 barg at the cathode, and an inlet water flow of 123 L min^{-1} on both sides, (b) specific heat according to the voltage overpotential.

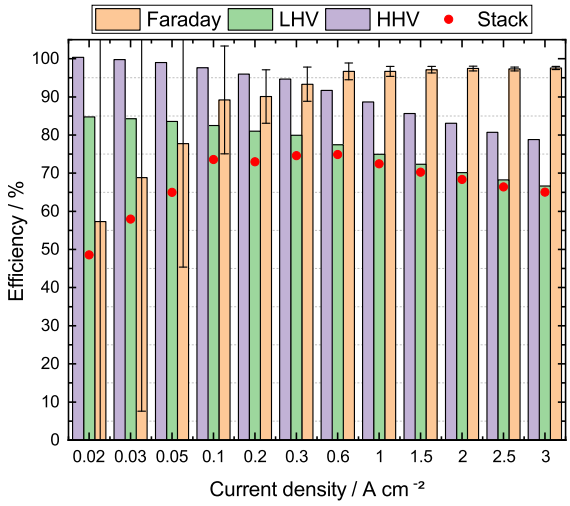

Fig. 7. Faraday and cell voltage efficiencies. Values above 100 % and below 0 % are not shown here, as they are not physically meaningful.

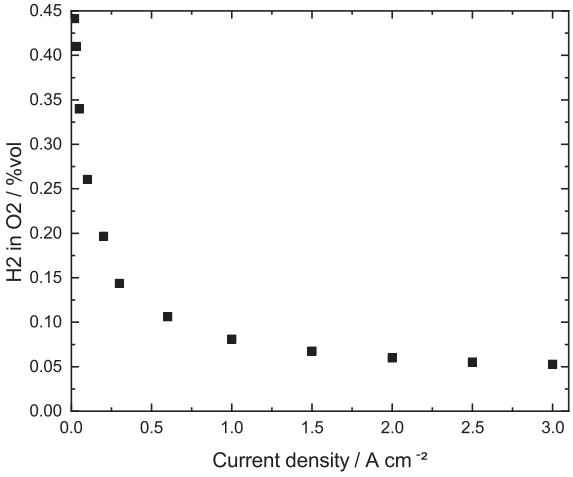

Fig. 8. H_2 in O_2 concentration for different current densities derived from the polarization curve at 70 °C, a pressure on the anode side of 4 barg and 5 barg on the cathode side and a water volume flow of 123 L min^{-1}.

the stack would change the convective heat loss across the surface, which would result in a greater heat flux heating the water. This would cause the temperature to rise and, consequently (due to the improved kinetics), the cell voltage to drop, which in turn would lead to a reduction in heat loss due to the decreased overvoltage, thereby reducing the heat input and the heating of the water, causing the cell voltage to rise again. It is therefore difficult to say at what value the cell voltage would stabilize without further experimental or numerical/analytical investigations.

In addition to stack efficiency, system efficiency is also of great importance for an industrial electrolyzer. We made a conscious decision not to specify an efficiency value for the system used here, as it is a test bench and not an industrial plant. To obtain the variety of information that forms the basis of this study, we implemented more actuators and sensors than are necessary for production.

As the definition of Faraday efficiency stipulates, the measured quantity of hydrogen is directly proportional to the theoretical quantity of hydrogen. As illustrated in Fig. 7, the efficiency consistently falls short of 100 %, indicating that a portion of the hydrogen produced must exit the stack via alternative pathways. The primary sink for this hydrogen is the crossover through the membrane to the anode side. Additional sinks include the sealing surface, and the gas dissolved in the water, which is subsequently drained off. It is imperative to note that the crossover process, if unchecked, has the potential to generate an explosive atmosphere within the anode chamber, particularly when the proportion of hydrogen in the oxygen flow attains and surpasses 4 %vol [26]. To avert such a scenario, the concentration of hydrogen in the oxygen flow, denoted as $c_{H_2 in O_2}$, is meticulously monitored and measured continuously. This measurement is depicted in Fig. 8. In accordance with the extant literature, the concentration of hydrogen in the oxygen flow exhibits an increase at low current densities and a decrease at higher current densities. The increased production of oxygen at higher current densities, dilutes hydrogen to a greater extent, resulting in a lower concentration. The stack, equipped with an integrated recombination catalyst layer [17], exhibits a concentration of 0.44 %vol at 0.02 A cm^{-2}, which decreases to 0.06 %vol at 3 A cm^{-2}. The authors are aware that continuous operation of an electrolyzer at 0.02 A cm^{-2} is not economical; however, given the fact that power generation can be volatile, operation may also be necessary in the low partial-load range, and safe operation is possible even at this operating point [26].

4. Conclusion

This contribution is about the beginning-of-life characterization of an industrial scale PEM electrolysis stack comprising 60 cells with 1024 cm^2

active area each. With polarization curve measurement and some additional sensors, it is possible to obtain comprehensive information about the stack operation.

It was found that for the investigated stack the optimal operating point in regard to minimal power consumption of $4.01\,\mathrm{kWh\,m^{-3}_{N,H_2}}$ and highest stack efficiency of 74.89 % (as a product of Faraday efficiency and LHV-related voltage efficiency) is at 1.61 V and $0.6\,\mathrm{A\,cm^{-2}}$. At the same operating point, the thermal system is at its equilibrium as no heating or cooling of the stack is needed. This aligns with analytical calculations in the literature showing that there is an optimal operating point. Based on this finding, stack operation at partial load is advantageous due to minimal OPEX. For very low electricity costs (e.g., direct coupling with renewable energy sources), the CAPEX might have a more pronounced share of the total costs. Besides the low power consumption, we achieved a mean cell voltage of 1.88 V at a current density of $3.0\,\mathrm{A\,cm^{-2}}$, which is quite impressive for a large scale stack.

For our stack we find significant differences in the single cell voltages at constant current. For $3.0\,\mathrm{A\,cm^{-2}}$, the voltage spread is 260 mV, which is the highest value along the polarization curve. Neglecting the outliers would lead to a 23 % lower voltage spread. Only a few cells operate at much higher voltages and thus at higher temperatures. Possible consequences include local hot spots and stack failure. When analyzing the possible reasons for the high voltage spread, we observe a strong correlation with the cathode-side contact resistance of the BPP. We find that in extreme cases the contact resistance can dominate the overall ohmic resistance of the cell. To minimize contact resistance, it is important to reduce the tolerances of the components and the assembly process to a minimum. Tolerances occur in component dimensions, coating quality and contact pressure. Assuming this has been done properly, the membrane resistance should account for the largest share of the ohmic resistance. In our case we find that a homogeneous and stable coating of the Ti BPP on both, the anode and cathode sides is necessary.

Finally, we observe a safe stack operation over the full range of current densities. Even at extreme partial loads much lower than $0.2\,\mathrm{A\,cm^{-2}}$ the hydrogen concentration on the anode side is far away from the explosion limit of 4 %vol. The recombination catalyst is doing a great job. The subsequent stage of the research would be to investigate transient operating conditions, such as start-ups, shutdowns, and dynamic behavior.

CRediT authorship contribution statement

Eugen Hoppe: Writing – original draft, Methodology, Formal analysis, Conceptualization. **Holger Janßen:** Writing – review & editing, Supervision, Formal analysis, Data curation. **Sebastian Holtwerth:** Writing – review & editing, Conceptualization. **Michael Hehemann:** Writing – review & editing, Data curation. **Walter Zwaygardt:** Writing – review & editing. **Martin Müller:** Writing – review & editing, Supervision, Funding acquisition, Conceptualization.

Declaration of competing interest

The authors declare the following financial interests/personal relationships which may be considered potential competing interests:

Eugen Hoppe reports that financial support was provided by the Federal Ministry of Research, Technology and Space. Holger Janssen has patent #EP000004128399B1 issued to Forschungszentrum Jülich GmbH. If there are other authors, they declare that they have no known competing financial interests or personal relationships that could have appeared to influence the work reported in this paper.

Acknowledgements

Funded by the Deutsche Forschungsgemeinschaft (DFG, German Research Foundation) - 491111487. The results of this work were achieved as part of the Living Lab Energy Campus project which demonstrates the intelligent coupling and model predictive control of integrated energy systems such as heat, electricity, chemical energy storage and conversion. It is funded by the Helmholtz Association. We would further like to thank Richard Wegner and Lukas Ritz for their tremendous help. The development of the BPP was partly supported by the H2Giga project PEP.IN (Grant No. 03HY120I).

Data availability

Data will be made available upon request.

References

[1] Höglinger M, Kartusch S, Eder J, Grabner B, Macherhammer M, Trattner A. Advanced testing methods for proton exchange membrane electrolysis stacks. Int J Hydrog Energy 2024;77:598–611. https://doi.org/10.1016/j.ijhydene.2024.06.118

[2] Lickert T, Fischer S, Young JL, Klose S, Franzetti I, Hahn D, Kang Z, Shviro M, Scheepers F, Carmo M, Smolinka T, Bender G, Metz S. Advances in benchmarking and round Robin testing for PEM water electrolysis: reference protocol and hardware. Appl Energy 2023;352. https://doi.org/10.1016/j.apenergy.2023.121898

[3] Liebert M, Joerissen L, Scholta J. Electrochemical impedance spectra measurements and analysis of polymer electrolyte membrane electrolysis on short stack. ECS Trans 2024;114:479–98. https://doi.org/10.1149/11405.0493ecst

[4] Badwal SPS, Giddey S, Ciacchi FT. Hydrogen and oxygen generation with polymer electrolyte membrane (PEM)-based electrolytic technology. Ionics 2006;12:7–14. https://doi.org/10.1007/s11581-006-0002-x

[5] Selamet F, Becerikli F, Mat MD, Kaplan Y. Development and testing of a highly efficient proton exchange membrane (PEM) electrolyzer stack. Int J Hydrog Energy 2011;36:11480–7. https://doi.org/10.1016/j.ijhydene.2011.01.129

[6] Santarelli M, Medina P, Calì M. Fitting regression model and experimental validation for a high-pressure PEM electrolyzer. Int J Hydrog Energy 2009;34:2519–30. https://doi.org/10.1016/j.ijhydene.2008.11.036

[7] Hancke R, Bujlo P, Holm T, Ulleberg Ă. High-pressure PEM water electrolyser performance up to 180 bar differential pressure. J Power Sources 2024;601. https://doi.org/10.1016/j.jpowsour.2024.234271

[8] Millet P, Ngameni R, Grigoriev SA, Mbemba N, Brisset F, Ranjbari A, Etiévant C. PEM water electrolyzers: from electrocatalysis to stack development. Int J Hydrog Energy 2010;35:5043–52. https://doi.org/10.1016/j.ijhydene.2009.09.015

[9] Wang J, Yang J, Feng Y, Hua J, Chen Z, Liao M, Zhang J, Qin J. Comparative experimental study of alkaline and proton exchange membrane water electrolysis for green hydrogen production. Appl Energy 2025;379. https://doi.org/10.1016/j.apenergy.2024.124936

[10] Kimmel B, Morawietz T, Gazdzicki P, Gago AS, Friedrich KA. Degradation mechanisms of a proton exchange membrane water electrolyzer stack operating at high current densities. Electrochim Acta 2025. https://doi.org/10.1016/j.electacta.2025.147395

[11] Emonts B, Müller M, Hehemann M, Janßen H, Keller R, Stähler M, Stähler A, Hagenmeyer V, Dittmeyer R, Pfeifer P, Waczowicz S, Rubin M, Munzke N, Kasselmann S. A holistic consideration of megawatt electrolysis as a key component of sector coupling. Energies 2022;15. https://doi.org/10.3390/en15103656

[12] Hoppe E, Janßen H, Holtwerth S, Müller M. FZJ 1056 CM^2 PEM electrolysis stack. JülichDATA 2025. https://doi.org/10.26165/JUELICH-DATA/IUF96L

[13] Müller M, Zwaygardt W, Janßen H, Holtwerth S, Behr W, Federmann D. Bipolar plate assembly, use of a bipolar plate assembly, and electrolysis or fuel cell stack comprising a plurality of bipolar plate assemblies. Patent EP000004128399B1 2023.

[14] Janßen H, Holtwerth S, Zwaygardt W, Stähler A, Behr W, Federmann D, Carmo M, Lehnert W, Müller M. A facile and economical approach to fabricate a single-piece bipolar plate for PEM electrolyzers. Int J Hydrog Energy 2024;49:816–28. https://doi.org/10.1016/j.ijhydene.2023.09.175

[15] Holtwerth S. Mechanisches verhalten von polymer-elektrolyt-membran-elektrolysezellen und -stacks, Energie & Umwelt. vol. 609. Jülich: Schriften Des Forschungszentrums Jülich; 2022. https://doi.org/10.18154/RWTH-2023-04311

[16] Burdzik A, Stähler M, Friedrich I, Carmo M, Stolten D. Homogeneity analysis of square meter-sized electrodes for PEM electrolysis and PEM fuel cells. J Coat Technol Res 2018;15:1423–32. https://doi.org/10.1007/s11998-018-0074-3

[17] Stähler A, Stähler M, Scheepers F, Lehnert W, Carmo M. Scalable implementation of recombination catalyst layers to mitigate gas crossover in PEM water electrolyzers. J Electrochem Soc 2022;169. https://doi.org/10.1149/1945-7111/ac5c9b

[18] Stähler M, Stähler A, Scheepers F, Carmo M, Stolten D. A completely slot die coated membrane electrode assembly. Int J Hydrog Energy 2019;44:7053–8. https://doi.org/10.1016/j.ijhydene.2019.02.016

[19] Moradi Nafchi F, Afshari E, Baniasadi E, Javani N. A parametric study of polymer membrane electrolyser performance, energy and exergy analyses. Int J Hydrog Energy 2019;44:18662–70. https://doi.org/10.1016/j.ijhydene.2018.11.081

[20] D. of Energy. Technical targets for PEM electrolyzer stacks and systems; 2026. https://www.energy.gov/cmei/fuels/technical-targets-proton-exchange-membrane-electrolysis.

[21] Hoppe E. Electrolyzer – polymer-electrolyte membrane electrolyzer | small and large scale units. vol. 6. 2025. p. 95–108. https://doi.org/10.1016/b978-0-323-96022-9.00220-6

[22] Qiu D, Janßen H, Peng L, Irmscher P, Lai X, Lehnert W. Electrical resistance and microstructure of typical gas diffusion layers for proton exchange membrane fuel

cell under compression. Appl Energy 2018;231:127–37. https://doi.org/10.1016/j.apenergy.2018.09.117
[23] Ito H, Maeda T, Nakano A, Takenaka H. Properties of nafion membranes under PEM water electrolysis conditions. Int J Hydrog Energy 2011;36:10527–40. https://doi.org/10.1016/j.ijhydene.2011.05.127
[24] Trinke P, Bensmann B, Hanke-Rauschenbach R. Current density effect on hydrogen permeation in PEM water electrolyzers. Int J Hydrog Energy 2017;42:14355–66. https://doi.org/10.1016/j.ijhydene.2017.03.231
[25] Scheepers F, Stähler M, Stähler A, Rauls E, Müller M, Carmo M, Lehnert W. Temperature optimization for improving polymer electrolyte membrane-water electrolysis system efficiency. Appl Energy 2021;283. https://doi.org/10.1016/j.apenergy.2020.116270
[26] Janssen H, Bringmann JC, Emonts B, Schroeder V. Safety-related studies on hydrogen production in high-pressure electrolysers. Int J Hydrog Energy 2004;29:759–70. https://doi.org/10.1016/j.ijhydene.2003.08.014